

Numerical and experimental analysis of two-dimensional separated flows over a flexible sail

By O. LORILLU, R. WEBER AND J. HUREAU

Laboratoire de Mécanique et d'Énergétique,
École Supérieure de l'Énergie et des Matériaux, Université d'Orléans,
8, Rue Léonard de Vinci, 45072 Orléans Cedex 2, France

(Received 27 November 2000 and in revised form 19 March 2002)

This paper is a numerical analysis of the flow over a flexible sail with the usual two-dimensional model of ideal weightless incompressible fluid. The sail is assumed to be impervious, inelastic and weightless, and may or may not be mounted on a mast. Separated or attached flows are considered at any angle of attack. Our method is validated by numerical and experimental results, i.e. the sail shape and velocity field are determined by particle imaging velocimetry, and lift and drag by aerodynamic balance. Despite the simplicity of the wake model we use (the Helmholtz model), the computed free streamline geometry and especially the sail shape are in good agreement with the experimental and numerical data.

1. Introduction

The fact that the shape of a sail will vary with the pressure on it makes sail aerodynamics more complicated than that of the ordinary thin airfoil. The static equilibrium of each sail element has to be included in the analysis, and the sail curvature has to satisfy both the static and dynamic equations.

1.1. *The literature*

The first model used to study two-dimensional sail aerodynamics for separated flows was proposed by Cisotti (1932). He considered a non-porous sail attached both at the leading (the 'luff') and the trailing (the 'leech') edges, with the flow separating at the sail's edges to form a quiescent wake. Dugan (1970) used Cisotti's model and the conformal mapping technique of Lévi-Civita (1907) to determine sail shapes and the aerodynamic forces on them. The nonlinear, singular integral equation resulting from the theoretical study is solved asymptotically for small deflections. Dugan initialized his solution with a flat plate of length L at an angle of attack α_0 . Moreover, he assumed that the tension T is constant along the entire sail, and justified this assumption by the lack of viscous shearing forces. For various angles of attack α_0 and tensions T , he found the shape of the sail, the positions of the leech and luff, and values of the drag and lift coefficients and the moment. Dugan's free streamline model is valid for a large range of angles of attack because the flow separates at the edges, contrary to the other models existing at that time, which concerned attached flows.

Voelz (1950) and Thwaites (1961) independently developed similar models for inelastic, flexible sails. Thwaites' formulation includes the effect of porosity, but the

numerical results are given only for non-porous sails. This model is the one most commonly referred to in the literature as the first relevant work on sail aerodynamics. The most important works published nowadays are based on these two models. In both, the sail is considered to have a distribution of vortices with the flow remaining attached over the whole sail. The aerodynamic model follows the classical linearized aerodynamic theory of rigid airfoils, assuming a small angle of attack, and includes an additional equation to be satisfied by the sail, i.e. that each element of the sail has to be in equilibrium. Again, the tension on the sail is taken as constant. Thwaites referred to the singular linear integro-differential equation for the strength of the vortex sheet resulting from the study as ‘*the sail equation*’. This is solved for a large number of flow configurations, for given sail length L , chord c (distance from leading to trailing edge), and angle of attack α between the chord and the free-stream velocity V_∞ . Voelz obtained the first eigenvalue of the integral equation and Thwaites generalized the result to higher eigenvalues, defined as a parameter λ :

$$\lambda = 2\rho V_\infty^2 c / T, \quad (1.1)$$

where ρ is the fluid density. The shape of the sail depends on this parameter. Thwaites determined that the resulting shape was wholly concave for $0 < \lambda < 2.316$ and would have one or more points of inflection for $\lambda \geq 2.316$. This value of 2.316 is very close to Voelz’s eigenvalue (2.299) and to the corresponding approximation of 2.310 given by Dugan (1970), who proceeded by way of a completely different theory.

Nielsen (1963) proposed a new mathematical solution based on Fourier series and numerical matrix techniques and using the simplified two-dimensional theory of thin airfoils established by Stewart (1942). He obtained similar results: with our notation, the sail shape is concave for $\lambda < 2.3155$. Irvine (1979) studied this problem of stability substituting a circular arc for the sail. He found that the sail remains concave up to the limit of $8/\pi \approx 2.547$. Moreover, the three models developed by Voelz, Thwaites and Nielsen generated numerical results in substantial agreement concerning the lift coefficient C_L , i.e. the lift force divided by $0.5\rho V_\infty^2 c$ (or $0.5\rho V_\infty^2 L$). They found that the sail’s lift coefficient is close to that of a flat plate, and differs only by a term depending on the excess length ratio of the sail ϵ ($\epsilon = (L - c) / c$):

$$C_L = 2\pi\alpha + A\sqrt{\epsilon}, \quad (1.2)$$

where the constant A is 6.36 for Thwaites and 7.2784 for Nielsen. All these works are valid only for small angles of attack, in contrast to Cisotti’s and Dugan’s models. Nielsen was the first to compare this expression with experimental results, although he does not show them: the differences between experiment and theory vary with the Reynolds number, sail camber and porosity.

The effect of porosity was studied in detail by Barakat (1968) and Murata & Tanaka (1989) who, following Thwaites’ theory for porous sails, present many results for the sail shape and the lift coefficient. Experiments were performed by Robert & Newman (1979) to determine the lift coefficient as a function of variations in incidence, Reynolds number and sail porosity. Newman & Low (1981) considered the same problem, but only at right angles, i.e. the case of parachutes. Sneyd (1984), following Nielsen’s theory, introduced yet another general sail parameter: its elasticity. The expression for the lift coefficient then depends on one more parameter (the coefficient of extensibility) and differs even more from the flat-plate expression. Jackson (1984) presented a general iterative method for inviscid two-dimensional flows around flexible, non-porous, inelastic sails. The pressure distribution is calculated for a given sail, and then the corresponding shape is found for this pressure distribution,

with the sail remaining at equilibrium. It should be noted that the tension on the sail, contrary to the other authors, is calculated and is not fixed as a given. Jackson's model is interesting because it can easily be adapted for less restrictive assumptions such as elastic sails (Jackson 1983), sails mounted on masts, or sails with surface friction.

Jackson & Christie (1987) developed a numerical method for the analysis of three-dimensional elastic membrane wings. This is an iterative process based on first finding the pressure distribution generated by a flow over a given three-dimensional surface (vortex lattice simulation of potential flow), and then finding the shape of a given membrane under a given pressure distribution (finite element representation of the membrane). An incremental formulation of the elastic membrane problem combined with a vortex lattice formulation of the thin-wing aerodynamic problem is also presented by Shyy (1997). Sugimoto (1996) examined a similar problem for flows around inextensible three-dimensional sails of high-aspect ratio and arbitrary planform. He combined lifting-line theory for the three-dimensional effects with thin-airfoil theory for the sectional aerodynamic characteristics. In using this latter theory, Sugimoto referred to the works of Voelz (1950) and Jackson (1983): the unknown camber of the two-dimensional sail is approximated by a cubic equation. It is not very significant to compare his result for total lift at high angles of attack because, in this theory, the flow remains attached.

More recently, Fitt & Lattimer (2000) described the motion of a two-dimensional inextensible sail at a small, time-dependent, angle of incidence in a uniform two-dimensional flow, basing their analysis on Voelz's theory. The shapes are determined for a given tension and different angles of attack (depending on the time), and their stability varies with the camber (the sign is not always the same). Nevertheless, even though authors tried to generalize their analysis of the flow around a sail by considering the sail porosity, elasticity, and flow steadiness, all these studies still apply only to attached flow over the whole sail.

Bundock (1980) and Vanden-Broeck (1982*a*) solved the fully nonlinear problem numerically using integral methods for inelastic non-porous sails. The model does not explicitly assume small angles of attack but, as Vanden-Broeck points out, 'it is not physical for α large since separation is then likely to occur'. Cyr & Newman (1996) proposed a new model to solve the flow over a non-porous, inextensible, flexible sail with rear separation. The method includes flow separation, which is determined by calculating the boundary layer on the sail, and is modelled by a single source on the sail surface near the trailing edge. The Kutta condition is applied to ensure realistic flow around the trailing edge. The solution is iterative. The numerical results are validated using experimental data obtained by the authors. This model is one of the few in the literature that includes separation on flexible sails: Wilkinson (1988) and Bailey, Jackson & Flay (1998) also studied the problem of the flow separating on the sail, even in the presence of a mast, but their methods are applied only to rigid sails. In both these studies, the sail and the mast are modelled by vortex and source sheets in the bubble regions (near the mast and leading edge where the flow separates and then reattaches) and in the wake near the trailing edge. Wilkinson's model considers non-viscous flows, while Bailey *et al.* consider the effects of viscosity on the calculated pressure distribution. Like Cyr & Newman, the free streamline geometry is not investigated.

Smith & Shyy (1995*a*) used new computation possibilities to study the problem of flexible two-dimensional membrane wings in steady laminar flow. The Reynolds number was then limited to 4000 and the flow determined using a Navier–Stokes

pressure based method. The equivalent case of unsteady laminar flow (the upstream velocity V_∞ varies periodically) was also studied with the same method (Smith & Shyy 1995*b*). This approach has been extended to turbulent flows (Smith & Shyy 1996) for Reynolds numbers of about 10^5 – 10^6 . The turbulence is modelled with a Navier–Stokes k – ω shear-stress transport eddy-viscosity model. The results were compared with classical inviscid membrane airfoil theory using vortex singularities to model the lifting potential flow around the airfoil, and were also compared with some experiments. The k – ω model was used because it can predict the position of the separation bubble for an inclined flat plate, unlike the k – ϵ model. The results are mixed: the potential theory is limited to incidences around the ideal, and to low viscous effects, while the results of the Navier–Stokes k – ω model differ from the experimental data (the authors suggested experimental difficulties). Lillberg, Kamakoti & Shyy (2000) continued to develop this numerical method by adding the effects of inertia to the dynamics of a flexible membrane both for laminar and turbulent unsteady flow fields.

These various models of attached or separated flows over flexible sails, sometimes considering porosity or elasticity, led to other studies on similar problems. Myall & Berger (1969) complemented these results by considering the interaction between a pair of two-dimensional sails. Tuck & Haselgrove (1972) and Vanden-Broeck & Keller (1981) studied a non-rigid attachment condition at the leech. Other configurations have also been analysed, such as double-membrane sails (Murai & Maruyama 1980) and inflated airfoils (Vanden-Broeck 1982*b*). All these authors considered that the flow was attached everywhere.

It is not always easy to make comparisons with the little experimental data published in the literature. It is very difficult, for example, to find attached flows around flexible sails experimentally; and what effect does the mast or the viscosity have in experiments? The sail's shape is rarely given either. Greenhalgh, Curtiss & Smith (1984) presented experimental variations of the aerodynamic and tension coefficients, C_D , C_L and C_T (non-dimensionalized, for the lift, by $0.5\rho V_\infty^2 c$), as a function of the angle of attack ($\alpha \in [-20^\circ; +20^\circ]$) for different excess length ratios ϵ (from 0.0021 to 0.0569 with our notation). Newman & Low (1984) gave equivalent results ($\epsilon \in [0.017; 0.1]$). The sail shape is given by the membrane angles at the trailing and leading edges, with the camber ratio and position. But what is of greatest interest in their experimental data is the position on the sail where the flow separates near the leading edge (bubbles) or trailing edge (wake). The experimental data from Cyr & Newman (1996) are for the aerodynamic coefficients with rear separation (with no bubble at the leading edge). As mentioned above, Robert & Newman (1979) presented experimental data for the effect of porosity on double-membrane sails, and Newman & Low (1981) on parachutes. In all these works, the mast at the leading edge is considered to be small enough to be neglected.

1.2. Method

The present paper deals with partially or fully separated flows as well as attached flows. The method presented here allows for the presence of a mast at the leading edge. Because the kind of flow we consider is different, our results differ from and complement those of the various authors cited above. The approach is first to consider the sail to be rigid and then to solve the typical problem of a curved obstacle with a thick wake (Hureau, Brunon & Legallais 1996) in order to find the pressure distribution on the sail and check if it has reached equilibrium. We then deform the

sail toward static equilibrium and repeat the method with this new shape until the sail has actually reached equilibrium.

The approach used here to solve the problem of determining the stationary, irrotational flow around a two-dimensional flexible sail differs from the other methods presented above, especially in the modelling assumptions used. First, we consider a sail with a thick wake, even though the flow remains attached over the whole sail, because the flow usually separates on the sail. Then, we use the Helmholtz model in which the wake pressure is set equal to the upstream pressure. In the numerical models presented above, the tension (λ or equivalent parameter) is set at the beginning of the iterative process. But there is no physical reason for doing this. Indeed, the sail tension corresponds more to a result of the calculations. How is the value chosen, then? In the method we present here, the given parameters are the chord c , the length L (or excess length ratio ϵ), the angle of incidence α of the chord with the upstream velocity V_∞ , and the mast geometry, if there is a mast. The positions of the separation points on the mast or sail must be given, but we are considering the possibility of coupling the numerical method with a boundary layer model to predict the point positions (this is not presented here). The object is mainly to find the sail geometry at equilibrium, and then the aerodynamic and tension forces.

We would like to point out that the assumption of constant wake pressure (Helmholtz model) is a crude one. However, it can be seen in sail pressure distributions (Cyr & Newman 1996) that it holds for the portion of the sail that is in the wake. So, since the problem concerns the investigation of the sail and the forces on it, the assumption is valid. The main problem with the Helmholtz model is the value to be assigned to the pressure ($P = P_\infty$, which is true only when the separation point is near the trailing edge). However, there are other wake models that result in a better prediction of the aerodynamic forces. The preliminary studies we present here seem to show that the pressure in the wake does not affect the sail shape greatly. In fact, this value seems to be important only for purposes of accuracy in predicting the aerodynamic and tension forces.

The method is based on conformal mapping techniques. The flow problem is not solved on the physical plane but on an auxiliary plane, i.e. inside the upper half-unit-disk, with the wetted part of the sail mapped on the half-circle. This conformal mapping method has already been used to solve other flow configurations such as impinging free jets (Hureau & Weber 1998), open channels and waterfalls (Toison & Hureau 2000), and two-dimensional flows around obstacles in a pipe (Weber & Hureau 2001). We wanted to use it here for this problem because the presence of the mast can then be considered, with flow separation everywhere on the sail. Unlike other authors' methods, ours holds for a wide range of angles of attack and excess length ratios. The computational requirements are quite small and the results, considering the assumptions made, are in rather good agreement with published and experimental results, as will be seen below. Moreover, this first approach is relatively easy to generalize to more complex sail flow configurations: it can be coupled with boundary layer calculations in order to define the position of separation points (see Legallais & Hureau 1994 for rigid obstacles); bubbles may be considered near the leading edge; other wake model can be used to model the wake pressure better and thus obtain better values for the aerodynamic forces; the interaction of two sails with attached or separated flows can be studied. All these possible applications are under consideration.

As with all new numerical methods, our computed results have to be validated. So, we conducted wind tunnel experiments to improve our computed sail shapes

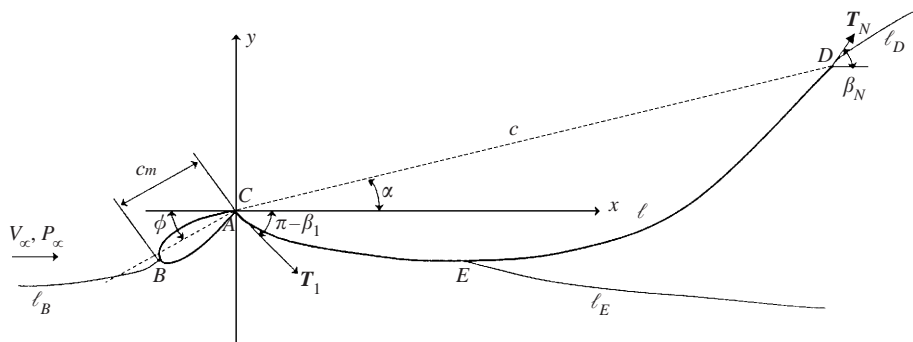


FIGURE 1. Notation.

in the presence of a mast because we know of no relevant results concerning such configurations in the literature. These validations consisted in determining the velocity field and sail shape using PIV instrumentation. Also, sails in the wind tunnel could be placed in an aerodynamic balance to compare the lift and drag coefficients, though it is well known that the Helmholtz model does not yield good agreement with experimental force measurements except when the pressure coefficient in the wake approaches zero, in which case the wake is not very large.

2. Solution

The sail shape and free streamline geometries are determined numerically. The problem is solved according to standard two-dimensional flow theory for ideal fluids.

2.1. Formulation

Let an obstacle consisting of a rigid mast (ABC) and flexible membrane be placed in a flow characterized by its velocity V_∞ along the horizontal x -axis and its pressure P_∞ (figure 1). The sail is assumed to be flexible, weightless, inelastic and impervious. We assume the fluid to be ideal, incompressible and weightless and the flow to be two-dimensional and irrotational and, indeed, permanent. The wake is quiescent (the Helmholtz thick model: $Cp = 0$) and the sail and the free streamline shapes are stationary.

The trailing edge of the sail is attached at point D , and the leading edge to the back of the mast at A . The mast, fixed at incidence ϕ , is thick but otherwise has an arbitrary profile that may be symmetrical but does not have to be, and its dimensions are usually small compared with those of the sail. The stagnation point is denoted B and the stagnation line ℓ_B . The trailing edge is always a separation point and another (assumed to be known) is denoted E . This can be either on the sail or on the mast, depending on the configuration. So, the wetted wall ℓ corresponds to $EABCD$. The length of ℓ is L . Free streamlines are denoted ℓ_E and ℓ_D ; c and c_m are the sail and the mast chords, respectively, and α is the angle between the sail's chord and the horizontal x . Lastly, let β be the angle between the tangent at some point on ℓ and the x -axis, and s the arclength starting from E .

Our purpose is to determine the geometry of free streamlines and the shape of the sail in (x, y) coordinates centred on the back of the mast. To solve this problem we used a recursive weighting scheme which can be applied to many different kinds of flows such as those mentioned above. According to the Helmholtz thick-wake model

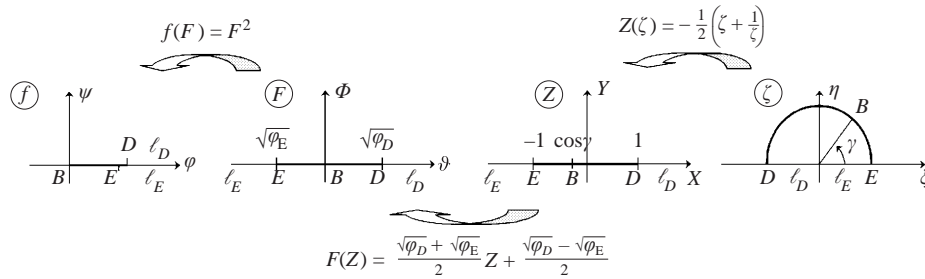


FIGURE 2. Conformal mapping of the f -plane onto the ζ -plane.

we used, the wake is assumed to be an infinite dead flow area and the pressure going into it is assumed to be P_∞ .

2.2. Theoretical formulation

The first step in our solution is to calculate the pressure forces on a sail with fixed shape, using the Helmholtz model.

Pressure forces on a rigid sail

We designate the position in the whole fluid flow domain by the complex variable z . Our aim is to define the complex potential $f(z)$ or the complex velocity $w(z) = df/dz$ in the whole fluid domain and the geometry of the free streamlines ℓ_E and ℓ_D using the relation $z = \int df/w$. The boundary conditions to be satisfied by the complex velocity can be written in the above notation (figure 1):

$$\lim_{z \rightarrow \infty} w(z) = V_\infty, \tag{2.1}$$

$$|w(z)| = V_\infty \quad \text{on} \quad \ell_E \cup \ell_D, \tag{2.2}$$

$$\text{Im}\{w(z) dz\} = 0 \quad \text{on} \quad \ell. \tag{2.3}$$

As a result of equation (2.2) and $\text{Arg}(w) = \beta$ on ℓ , we have a mixed problem for a particular function Ω defined as

$$\Omega = -i \log(V_\infty/w) = \Theta + iT. \tag{2.4}$$

The usual method for solving this problem was introduced by Lévi-Civita (1907) and consists in reducing the mixed problem to a Dirichlet problem. The physical plane (z) is mapped on the inside of the upper unit semi-circle, in such a way that free streamlines map onto the diameter and ℓ onto the semi-circle (figure 2). With (2.2) we have $T = 0$ on the diameter and thus Ω can, according to Schwarz's principle of symmetry, be continued inside the whole disk. If we assume we know the one-to-one correspondence between ℓ into (z) and ℓ into (ζ), then we know the real part of Ω on the unit circle from the geometry of ℓ . Therefore the mixed problem becomes a Dirichlet problem and we use the Schwarz–Villat formula to determine Ω entirely (Muskhelishvili 1977).

The singularity of the flow at the stagnation point is isolated by expressing Ω on the upper semi-circle in terms of $\theta(\sigma) = \Theta(\zeta)$ and $\tau(\sigma) = T(\zeta)$:

$$\Omega(\sigma) = \theta(\sigma) + i\tau(\sigma) = \Omega_S(\sigma) + \tilde{\Omega}(\sigma), \tag{2.5}$$

where Ω_S is a particular solution having the same singularity as Ω , $\tilde{\Omega}$ is a regular

function, and σ is the angle describing the position of a point moving along the semi-circle ($\zeta = e^{i\sigma}$). The singularity function Ω_S may be written as a flat-plate function (Gurevich 1966):

$$\Omega_S(\sigma) = \theta_S(\sigma) + i\tau_S(\sigma) = -3\pi/2 + \gamma + i \log \left(\frac{e^{i\sigma} - e^{i\gamma}}{e^{i\sigma} - e^{-i\gamma}} \right), \quad (2.6)$$

where γ is the position of the stagnation point in the ζ -plane.

Next we solve the Dirichlet problem for the regular function $\tilde{\Omega}(\sigma) = \tilde{\theta}(\sigma) + i\tilde{\tau}(\sigma)$. If we denote the one-to-one boundary correspondence function as $\epsilon_\ell : \sigma \in [0; \pi] \rightarrow s \in [0; L]$, then $\tilde{\theta}$ is defined from the geometry of the contour:

$$\tilde{\theta}(\sigma) = (\beta \circ \epsilon_\ell)(\sigma) - \pi/2, \quad \forall \sigma \in [0; \pi]. \quad (2.7)$$

The angle defining the position of the stagnation point on the auxiliary plane, γ , is calculated. Considering (2.1), we have $\Omega(0) = 0$ and hence

$$\gamma = \frac{\pi}{2} + \frac{1}{\pi} \int_0^\pi \tilde{\theta}(\sigma') d\sigma'. \quad (2.8)$$

The function $\tilde{\tau}$ is determined by the Schwarz–Villat formula (Muskhelishvili 1977) which can be written on the semi-circle:

$$\tilde{\tau}(\sigma) = \frac{1}{\pi} \lim_{\zeta \rightarrow e^{i\sigma}} \left(\text{Im} \left\{ \int_0^\pi \tilde{\theta}(\sigma') \frac{1 - \zeta^2}{1 - 2\zeta \cos \sigma' + \zeta^2} d\sigma' \right\} \right). \quad (2.9)$$

With (2.7), (2.8) and (2.9), Ω and consequently $w(z)$ are known throughout the fluid domain. Next, in order to calculate the function $\epsilon_\ell(\sigma)$, which we have assumed to be known up to now, we need to know the complex potential f . This is done by conformal mapping of the potential plane (f) onto the auxiliary plane (ζ) as in Gurevich (1966) and Milne-Thomson (1968) (figure 2).

From figure 2, we obtain the relation between the potential plane and the auxiliary plane, where a is a constant to be determined:

$$f(\zeta) = a^2 \left[\cos \gamma - \frac{1}{2} \left(\zeta + \frac{1}{\zeta} \right) \right]^2. \quad (2.10)$$

With (2.4) we can define the variation of position dz on the physical boundaries of the flow:

$$dz = \frac{2a^2}{V_\infty} e^{i\theta(\sigma)} e^{-\tau(\sigma)} (\cos \gamma - \cos \sigma) \sin \sigma d\sigma. \quad (2.11)$$

The function ϵ_ℓ can therefore be determined using the variation of arclength ($ds = |dz|$) and (2.11). Thus, with $\epsilon_\ell(\pi) = L$, from which we determine the constant a , we obtain the function ϵ_ℓ :

$$\epsilon_\ell(\sigma) = L \frac{G(\sigma, \gamma)}{G(\pi, \gamma)} \quad \text{where} \quad G(\sigma, \gamma) = \int_0^\sigma 2 \frac{\sin \sigma'}{e^{\tilde{\tau}(\sigma')}} \sin^2 \left(\frac{\sigma' + \gamma}{2} \right) d\sigma'. \quad (2.12)$$

Lastly, this sequence can be repeated using this new distribution ϵ_ℓ , beginning with (2.5) and continuing until convergence. Next, we can calculate the distribution of the pressure coefficient on the sail in order to verify the static equilibrium with the following formula:

$$Cp(\sigma) = 1 - e^{2\tilde{\tau}(\sigma)} \left| \frac{\sin((\sigma - \gamma)/2)}{\sin((\sigma + \gamma)/2)} \right|^2. \quad (2.13)$$

We can determine the modulus of the pressure force $\mathbf{F}p_i$ acting on a small element ds_i of the wetted wall (mast or sail) at the middle \tilde{s}_i of a segment of sail comprising $N - 1$ such segments, using the pressure coefficient (2.13) and the correspondence function ϵ_ℓ :

$$\|\mathbf{F}p_i\| = \frac{1}{2}\rho V_\infty^2 C_p(\tilde{s}_i) ds_i. \quad (2.14)$$

Thus we can calculate the total pressure force acting on the whole sail by $\mathbf{F}p = \sum \mathbf{F}p_i$.

Sail equilibrium and deformation

In order to verify the equilibrium on each sail segment, we need to know the expression for the reaction forces \mathbf{T}_1 and \mathbf{T}_N on the attached points C and D . The fundamental relation of the dynamics give

$$\mathbf{T}_1 + \mathbf{T}_N + \mathbf{F}p = 0. \quad (2.15)$$

Since we know the angles β_1 and β_N from the shape of the sail, reaction forces \mathbf{T}_1 and \mathbf{T}_N are entirely determined.

Now, we must apply an equilibrium condition on each middle point \tilde{s}_i of a segment. Obviously, we do not conduct these calculations on the mast but only on the flexible sail. The equilibrium of the middle point may be written as the equality of the forces \mathbf{F}_{bef} and \mathbf{F}_{aft} acting on all sides:

$$\mathbf{F}_{bef} = \mathbf{T}_1 + \sum_{k=1}^{i-1} \mathbf{F}p_k + \frac{1}{2}\mathbf{F}p_i \quad \text{and} \quad \mathbf{F}_{aft} = \frac{1}{2}\mathbf{F}p_i + \sum_{k=i+1}^{N-1} \mathbf{F}p_k + \mathbf{T}_N. \quad (2.16)$$

It can be seen that, by definition, these two forces have the same direction and length and are opposed to each other. When the sail has reached equilibrium, the direction of these forces is the same as the tangent at the point \tilde{s}_i . However, this is not true in an ordinary iteration of the system, unless converged. Therefore, a new distribution of β_i can now be determined on the sail in order to approach equilibrium. We introduce a weighting factor r_s with the intention of not modifying the segment angle too quickly:

$$\beta_i^{\text{new}} = r_s \beta_i^{\text{old}} + (1 - r_s) \tilde{\beta}, \quad (2.17)$$

where $\tilde{\beta}$ is the angle of the force \mathbf{F}_{aft} with the x -axis. With this new tangent distribution and with the arclength distribution, a new sail shape can now be determined. However, the trailing edge has moved with this modification and thus we must adjust the shape to restore it. This is done by moving all the points by the same step and, respectively, along the x - and y -axes. This global replacement changes the length of the sail, so we must now adjust it to the real initial length. This stage is especially difficult because the curvature of the sail has to be changed as little as possible. To do this, we consider three consecutive points s_{i-1} , s_i , and s_{i+1} and move the central one along the perpendicular of the segment $[s_{i-1}; s_{i+1}]$ which is drawn from s_i . We then compute the new coordinates.

We now have a new sail shape with the trailing edge at its initial position and the sail at its real length. The method can be repeated with this new shape, beginning with the computation of pressure forces on the rigid sail.

2.3. Without a mast

As mentioned in the introduction, one of the aims of this work is to treat the case of flow around sails with a mast. But most of the data available for sails in the literature do not take a mast into account. To compare our results, we have to treat

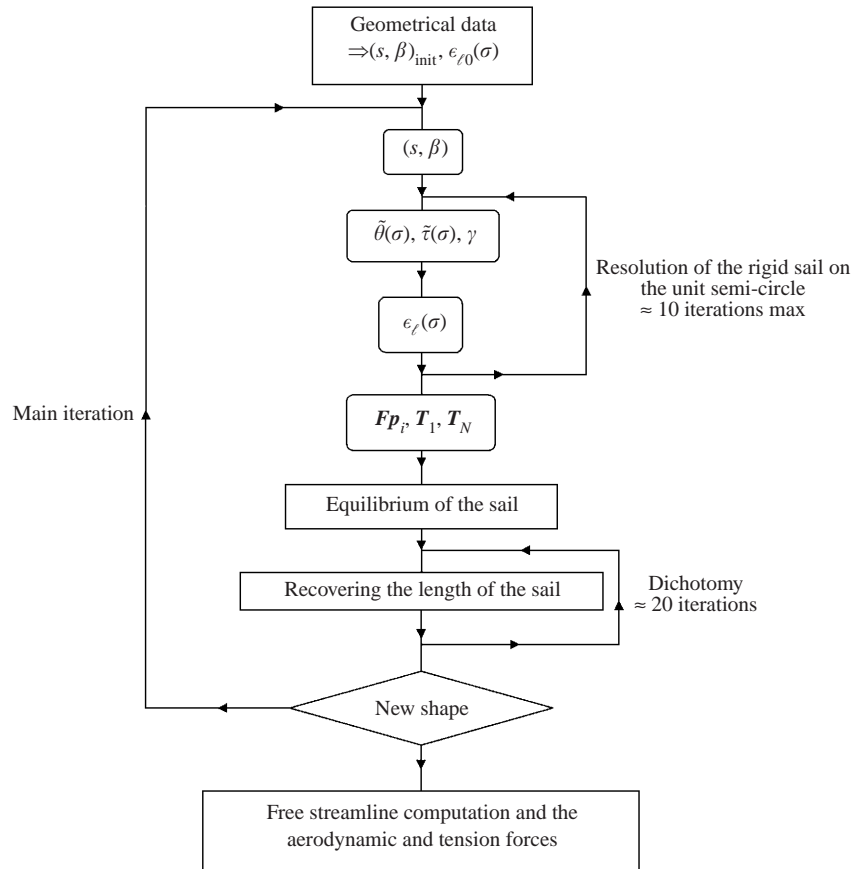


FIGURE 3. Algorithm.

the problem with the sail only. A singularity is thus introduced at the leading edge (the velocity becomes infinite at this point):

$$\Omega_{S_{le}}(\sigma) = -i \log \left(\frac{e^{i\sigma} - e^{i\gamma_{le}}}{e^{i\sigma} - e^{-i\gamma_{le}}} \right), \quad (2.18)$$

where γ_{le} is the angle defining the position of the leading edge in the ζ -plane. This singularity is added to the singular function Ω_S , and the numerical problem is then solved in the same way.

The numerical solution of the problem is presented in the next section only for the case of a sail with a mast. It will also be found that a very small mast can be used, instead of introducing this supplementary singularity at the leading edge.

Note that with this method, the sail is required to be at design incidence.

2.4. Numerical solution

The unknowns of the problem are the functions $\sigma \mapsto \tilde{\theta}(\sigma)$, $\sigma \mapsto \tilde{z}(\sigma)$, $\sigma \mapsto \epsilon_\ell(\sigma)$ for $\sigma \in [0; \pi]$, the position of the stagnation point B on the unit semi-circle of the ζ -plane (γ), and the shape of the sail characterized by the distribution of arclengths and tangents (s, β) .

The solution is obtained numerically using the recursive algorithm described in

figure 3. The three steps are the initialization, the chief iteration, and finally the exit from the iterative system when a convergence criterion is met.

Initialization

The problem is first defined geometrically in terms of mast position and profile, position of extremities, sail length, and flow separation point position, which is needed for our method. Next, the initial sail geometry is defined. This can be based on a parabola, a sinusoidal curve, or a circular arc, for example. The initial (s, β) pair of the sail is computed. The semi-circle is divided into N_c equally spaced points between 0 and π . We next have to define the initial function ϵ_ℓ . Here we usually choose a linear function with $\epsilon_\ell(0) = 0$ and $\epsilon_\ell(\pi) = L$.

Chief iteration

First, the pressure forces are computed. To do this, we solve the system of equations (2.7), (2.8), (2.9) and (2.12) using the (2.19) recursive weighting algorithm:

$$\left. \begin{aligned} \epsilon_{\ell n} &= (1 - r_{\epsilon_\ell})f_{\epsilon_\ell}(\tilde{\tau}_{n-1}, \gamma_{n-1}) + r_{\epsilon_\ell}\epsilon_{\ell n-1}, \\ \tilde{\theta}_n &= (1 - r_{\tilde{\theta}})f_{\tilde{\theta}}(\epsilon_{\ell n-1}) + r_{\tilde{\theta}}\tilde{\theta}_{n-1}, \\ \gamma_n &= (1 - r_\gamma)f_\gamma(\tilde{\theta}_{n-1}) + r_\gamma\gamma_{n-1}, \\ \tilde{\tau}_n &= (1 - r_{\tilde{\tau}})f_{\tilde{\tau}}(\tilde{\theta}_{n-1}) + r_{\tilde{\tau}}\tilde{\tau}_{n-1}, \end{aligned} \right\} \quad (2.19)$$

where r_{ϵ_ℓ} , $r_{\tilde{\theta}}$, r_γ and $r_{\tilde{\tau}}$ are four weighting factors belonging to $[0; 1]$, usually chosen as $r_{\epsilon_\ell} = 0.9$, $r_{\tilde{\theta}} = 0.5$, $r_\gamma = 0$, and $r_{\tilde{\tau}} = 0.5$.

The integrals of the three equations (2.12), (2.9) and (2.8) are solved by a numerical scheme such as the trapezoidal rule. Several iterations of (2.19) are needed to stabilize the position of the stagnation point (γ), but it is never necessary to go as far as the convergence of (2.19), since the sail shape is not the final one. We usually follow the following rule: the closer we come to the final sail shape, the more often the subsystem (2.19) should be repeated, with a limit of around ten iterations.

Then, we compute the pressure coefficient distribution with (2.13) to find the pressure forces on each point of the sail with (2.14), the reaction forces, and the resultant forces on each middle point of the sail with (2.16).

The last stage of the main iteration is to deform the sail by (2.17) in order to apply the equilibrium condition smoothly, then relocate the trailing edge position. Usually (2.17) is computed with a weighting factor r_s of about 0.5 but, when the sail is very much longer than its chord c , this factor can go as high as 0.9.

Then, we deform the sail smoothly again in order to return to the true length. To do this, we construct a function varying from 0 to 1, in order to move the extreme points of the sail by less than the centre. The difference between the sail's current and real length is dichotomized. Usually this stage requires ten or twenty iterations with a precision of 10^{-4} in the length.

Exit from the global system

The main iteration is repeated up to convergence, which is reached when the mean difference between sail tangents and resultant pressure forces (2.16) is less than the precision fixed by user. After exiting from the subsystem, we plot free streamlines ℓ_E and ℓ_D by integrating dz over the diameter of the semi-circle of the ζ -plane, and plot the pressure distribution on the sail with (2.13). We calculate the global lift and drag coefficients with the pressure integration rule or Blasius' formula (Gurevich 1966).

3. Experimental setup

As explained in the introduction, there is too little in the literature concerning flows over two-dimensional impervious flexible sails with a mast to compare our numerical calculations. So, we performed experiments in a wind tunnel to study the sail shape and determine the aerodynamic forces. Nevertheless, most of the calculations would be improved by comparison with numerical or experimental results.

3.1. Wind tunnel

All experiments were performed in the Lucien Malavard wind tunnel. This is a subsonic closed-circuit wind tunnel with a square ($2\text{ m} \times 2\text{ m}$) test section, 5 m long. A 265 kW electric fan generates a maximum velocity of 60 m s^{-1} in the open test section. The mean turbulence ratio measured in this section without an obstacle is 0.4%. Two flat plates ($2\text{ m} \times 4\text{ m}$) can be installed to limit three-dimensional effects. The obstacle is installed on two disks (1 m in diameter) which rotate to place the obstacle at the desired incidence. The disks can be mounted on an aerodynamic balance fitted under the tunnel floor. This is a six-component balance, but only the lift and drag forces are measured here. One of the disks is transparent, for direct visualizations and video acquisitions, and the laser sheet enters the wind tunnel section through the floor.

3.2. Particle image velocimetry (PIV) system

The experimental data generated are the two-dimensional components of the velocity around the obstacle. In most PIV applications, the flow is seeded with tracer particles. In our case, an oil generator is used to generate and supply particles (the oil is vaporized on an electric resistor). The mean diameter of the particles is about $1\text{ }\mu\text{m}$. The tracer particle generator is placed just in front the honeycomb at the beginning of the wind tunnel convergent section. The laser sheet is generated by a double-oscillator laser. Here, we used a Nd:Yag laser (Spectra Physics 400) adjusted on the second harmonic and emitting two pulses of 200 mJ each ($\lambda = 532\text{ nm}$), at a repetition rate of 10 Hz. The laser sheet is developed with the usual laser sheet optics, with mirrors and spherical and cylindrical lenses with negative and positive focal lengths. For reasons of limited space, the mirrors are mounted on an optical arm with lenses to obtain a laser sheet with a divergence of about 60° and a thickness of about 1 mm around the obstacle. For the experimental data presented here, the images are obtained by a CCD camera with 1008×1016 sensor elements (camera CCD PIVCAM) placed perpendicularly to the laser sheet and in the direction of a section of the two-dimensional obstacle. The laser pulses are synchronized with the image acquisition by a TSI synchroniser system driven by InSight-NTTM software. For all the data presented in this paper, the PIV recordings are divided into small interrogation areas corresponding to 32×32 pixels. In the data post-processing, the interrogation areas overlap by 50%, which corresponds to defining 61×62 vectors on the visualized area. The local displacement vector is determined for each interrogation area by statistical methods (auto-correlation). The projection of the local flow velocity vector onto the laser sheet plane is calculated by InSight using the time delay between the two illuminations (Δt) and the magnification at imaging.

3.3. Sail and mast

We performed several experiments in which the sail length, chord and incidence were changed to move the separation point farther from or closer to the mast, or onto the mast. The sail was made of impervious nylon that is light enough to be considered weightless, and rigid enough to be considered inelastic. In fact, the

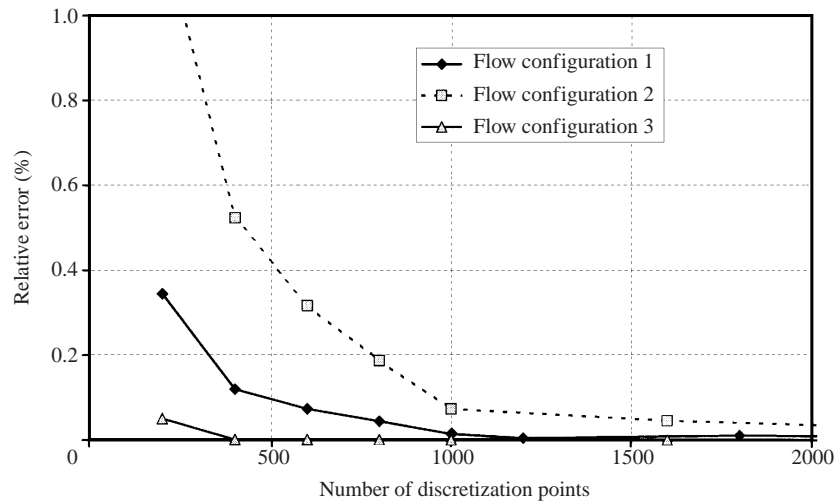


FIGURE 4. Influence of the discretization step on the computed lift coefficient; $\epsilon = 0.1$, $\alpha = 15^\circ$, $c_m = 0.1$ mm (NACA0060 profile) and $s/c = 0.401$ for flow configuration 1; $\epsilon = 0.03$, $\alpha = 12.5^\circ$, $c_m = 0.03$ mm (NACA0060 profile) and $s/c = 0.613$ for flow configuration 2; and $\epsilon = 0.05$, $\alpha = 30^\circ$, and the flow is fully separated for flow configuration 3.

fabric was doubled to prevent any porosity effects. The masts used were symmetrical NACA0040 or NACA0060 profiles. A thin steel wire (about 1.5 mm diameter) runs along the trailing edge and is attached to the disks at very high tension to reduce the bending under the load on the sail, while allowing the sail to be weighed. PIV visualization gives us the position of the separation point, which is what we need to solve the problem.

4. Results

We now present some numerical results computed with our method, beginning with some results showing its limitations and possibilities. We will then try to validate our results by comparison with published data or some of our own experimental results for attached and separated flow configurations without a mast. Lastly, the general configurations with a mast and separated flows are validated with our PIV experiments.

4.1. First numerical results

The number of discretization points in the ζ -plane is a very important parameter for the quality of the computed results. Many trials have been performed on several flow configurations to test the influence of this parameter. It was found that the computed aerodynamic coefficients vary little at convergence as the number of points on the sail increases for a given configuration—shape, mast discretization and incidence, chord, sail incidence and excess length ratio and the position of the separation points are fixed. Figure 4 shows the relative error on the computed lift coefficient obtained at convergence for different discretization steps on the semi-circle for three flow configurations (fully or partially separated flows, different mast sizes and excess length ratios) as a function of the number of discretization points. The reference value is taken equal to the coefficient calculated for 3601 points on the semi-circle. For the computed results we present in this paper, the convergence criterion defined

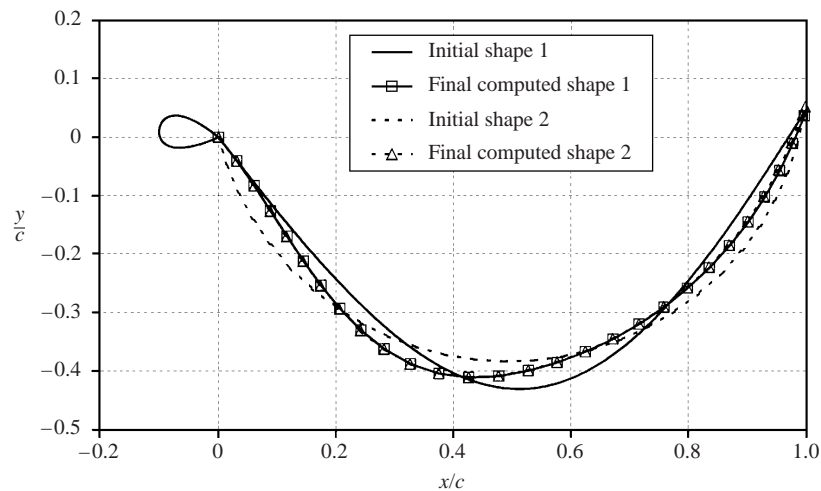


FIGURE 5. Influence of the initial sail shape on the converged result; $\epsilon = 0.4$, $\alpha = 3^\circ$. The first initial shape is sinusoidal and the second is an arc of a circle. The separation point is fixed at the sail midpoint ($s/c = 0.7$).

at the end of §2.4 will always be less than 0.5° , but most of the time it will be about 0.05° . It should be noted that increasing the number of discretization points will increase the accuracy and decrease the convergence criterion, but the calculation time will increase quickly from a few seconds (on a PC 500 MHz) for fully separated flows and some 300 points on the semi-circle to some hours for partially separated flows and 3601 points. A good compromise between accuracy and computation time is about 400 discretization points on the sail, and convergence is reached in a total computation time of a few minutes at most, with less than 0.5% relative error in the lift coefficient (figure 4).

Another parameter that might affect the results is the initial sail shape. The numerical method is therefore initialized with two different sail shapes (first sinusoidal and then a circular arc) with the same mast geometry and incidence in both cases. The final shapes we found are presented in figure 5 with symbols. They are indistinguishable. This test was performed on a number of different configurations (more realistic flow configurations), and the results were always the same. So, it can be said that the numerical method is valid for any initial sail shape. The configuration in figure 5 is not a realistic case for sailing because the excess length ratio is very large ($\epsilon = 0.4$) and the incidence of the sail is small ($\alpha = 3^\circ$), but this example was chosen to show the ability of our method to find even curious shapes. An inflection point can be seen at the luff. This has been observed for other configurations ($\epsilon \geq 0.1$ and α small), but it is not possible to compare the parameter λ (1.1) found here with the values given by Thwaites (1961) and others because their theories are valid only for attached flows with no mast. Here, we have general flow configurations with partially separated flows and a mast at the luff.

Another case used to test the possibilities of our method is the symmetrical flow configuration, as in parachutes or bluff membranes. The incidence of the sail is then 90° , the flow separates at the trailing and leading edges, and there is no mast. Figure 6 gives our computed results (solid and broken lines) for three different excess length ratios: 0.01, 0.15 and 0.5. Large ratios are not exceptional in these kinds of applications. Newman & Low (1981) and Newman (1987), consider circular arc

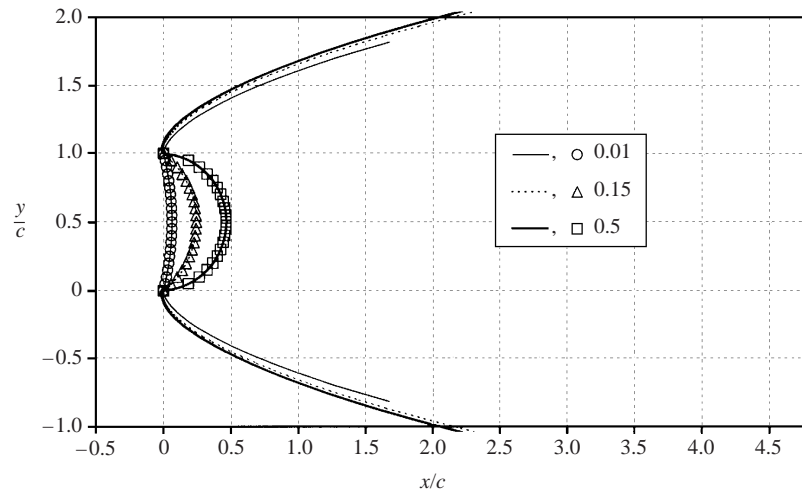


FIGURE 6. Symmetrical shape (parachutes) and free streamlines for different ϵ . The lines corresponds to the computed results and the symbols to circular arcs.

shapes of slightly porous sails. The shapes presented in figure 6 were obtained from an initial sinusoidal shape. The symbols represent circular arcs of lengths $1.01c$, $1.15c$ and $1.5c$. Very good agreement can be seen between our results and the assumption of an arc of a circle.

Unlike other authors, we do not assume that the tension is constant in the sail. It should be said, though, that the tension as we calculated it does tend to be constant anyway, and the reactions $\|\mathbf{T}_1\|$ and $\|\mathbf{T}_N\|$ have to be equal. For the above sail of length $1.5c$, we find a mean value of 0.499 for the tension coefficient C_T in the sail, and less than 0.18% variation around this value, while we obtain a mean of 0.631 for the $1.15c$ sail, and less than 0.02% variation. We can say here that the tension coefficient is found to be constant in each case, and thus validates the numerical method. Moreover, we notice that the greater the excess length ratio, the greater the percentage of variation around the mean value for a given convergence criterion. Nevertheless, this variation is always less than 0.5% at convergence.

Lastly, the presence of a mast will change the sail configuration because the separation point moves from the sail to the mast as the incidence ϕ decreases and becomes negative. Moreover, considering the formulation without a mast (but with the additional singularity (2.18)) or the 'classical' configuration with a very small mast of chord one hundred or one thousand times smaller than the sail chord produces equivalent results if there are enough discretization points.

4.2. Attached flows

As mentioned in the introduction, many theories have been developed for studying attached flow around a flexible sail without a mast (Voelz 1950; Thwaites 1961; Nielsen 1963 or Vanden-Broeck 1982a, for example). So, this configuration is a good one for validating our computations. Nevertheless, our method differs from those mentioned above because of the assumed thick wake. The flow remains attached on the whole sail and a thick wake appears behind the sail. The smaller the sail's angle of incidence, the longer the two free streamlines determining the wake are superimposed. The theories of Voelz, Thwaites and Nielsen all state that the function C_L/α varies only with the parameter $\alpha/\sqrt{\epsilon}$ (1.2). This is why only one theoretical

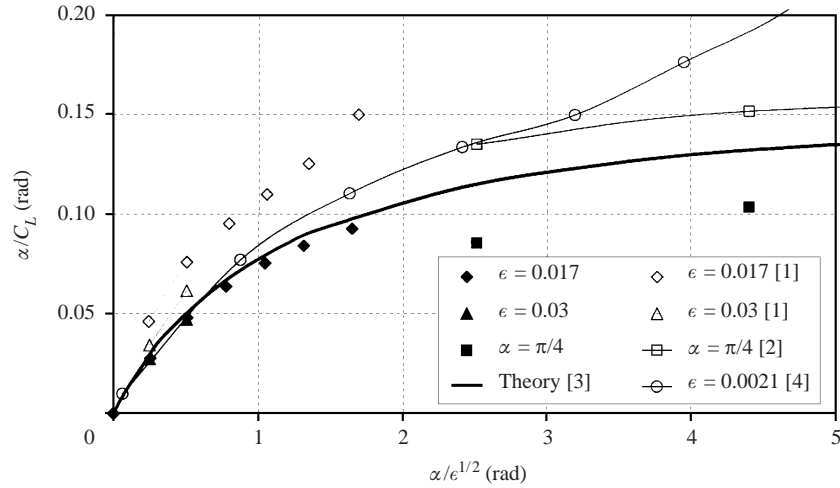


FIGURE 7. Lift coefficient. Comparison between computed results (solid symbols) and published results (open symbols, from [1] Newman & Low (1984), [2] Vanden-Broeck (1982a) and [4] Greenhalgh *et al.* (1984)) and theory ([3] Nielsen (1963)).

	C_D		C_L	
	Dugan (1970)	Present method	Dugan (1970)	Present method
$\epsilon = 0.001, \alpha = 8.5^\circ$			0.2777	0.2800
$\epsilon = 0.010, \alpha = 11^\circ$	0.0747	0.0751	0.4579	0.4505
$\epsilon = 0.090, \alpha = 16.5^\circ$	0.1821	0.1813	0.6893	0.6882

TABLE 1. Aerodynamic coefficients for a fully separated sail, non-dimensionalized by L .

curve is represented in figure 7. Experimental data for this flow configuration are given by Newman & Low (1984) and Greenhalgh *et al.* (1984). It should be noted that it is very difficult to achieve attached flows experimentally because the flow will separate on the sail if the excess length ratio or the incidence are too large. Indeed, Newman & Low showed that bubbles usually appeared near the leading edge. This was probably true for Greenhalgh *et al.* too, but the problem was not addressed. The presence of these bubbles could explain the differences between experiment and theory. Our computed results are in good agreement with the theory as long as the ratio $\alpha/\sqrt{\epsilon}$ is not too large (figure 7), though less so with experimental results. The sail shapes correspond very well too (figure 8). These results are not surprising because the thick wake assumption of the Helmholtz model is quite exact in the case of flows that remain attached.

This assumption of attached flow is valid only for small angles of attack, small excess length ratios, and no large negative angles for the mast if there is one. In all the other configurations, the flow will separate on the sail (or the mast), so comparisons with the theories of Thwaites or Voelz are not valid for large angles α or ratios ϵ .

4.3. Partially or fully separated flows

The opposite of attached flows are fully separated flows: the flow separates both at the leading and the trailing edges. We then have the configuration studied by Dugan (1970). Even though Dugan's numerical method is not the same as ours, we see a very

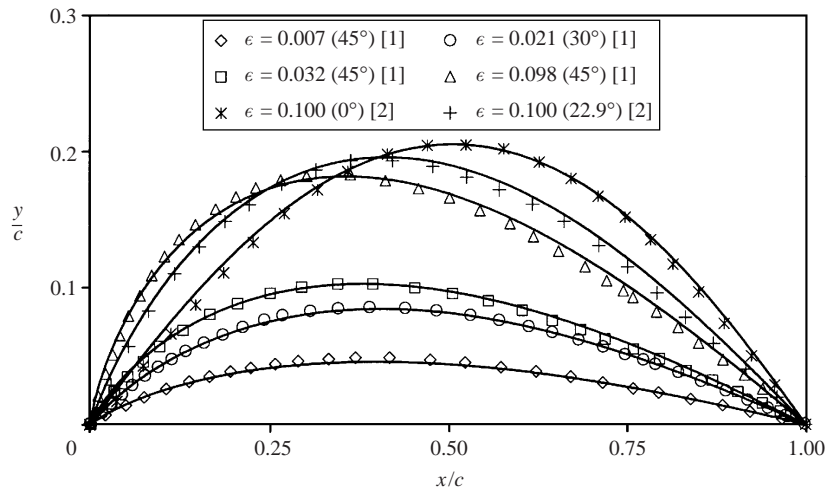


FIGURE 8. Sail shape. Comparison between computed results (lines) and results from the literature (with symbols [1] for Vanden-Broeck (1982a) and [2] for Jackson (1984)).

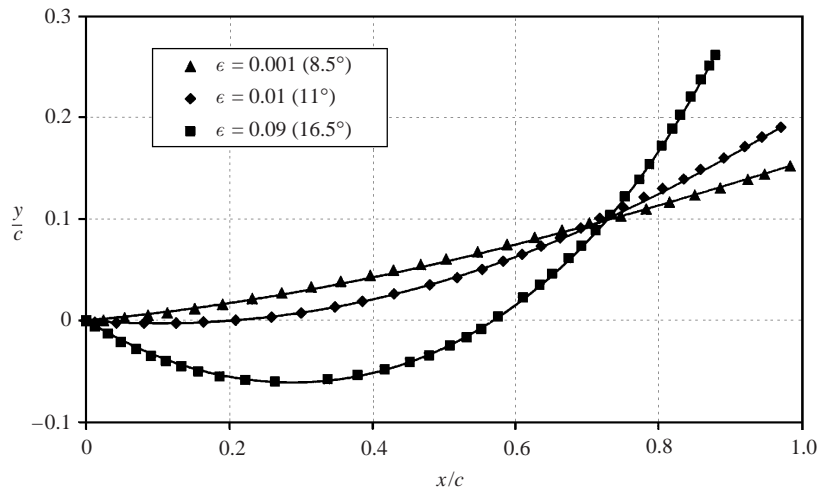


FIGURE 9. Comparison of the computed sail shape (lines) with the results of Dugan (1970) (symbols) for fully separated flows.

good correspondence in the results for the aerodynamic coefficients and sail shape (table 1 and figure 9). Once again, these results are expected because the wake model used is the same. Newman & Low (1984) have experimental data for fully separated flows, giving the aerodynamic coefficients (ratio C_L/C_D) up to the point where the flow separates at the leading edge. Subsequent increases in the angle of incidence do not change the flow configuration (figure 10). To complete the study of this configuration, we performed some experiments in the Lucien Malavard wind tunnel to measure the aerodynamic forces on a sail with a balance, for a large incidence range and two different sails ($\epsilon = 0.08$ and 0.23 , see table 2 in the next section, configuration 4). Some of these results are reported in figure 10 along with the corresponding results generated by our numerical method. For each experimental point corresponding to a fully separated flow, the equivalent computed point is shown. It can be seen that the

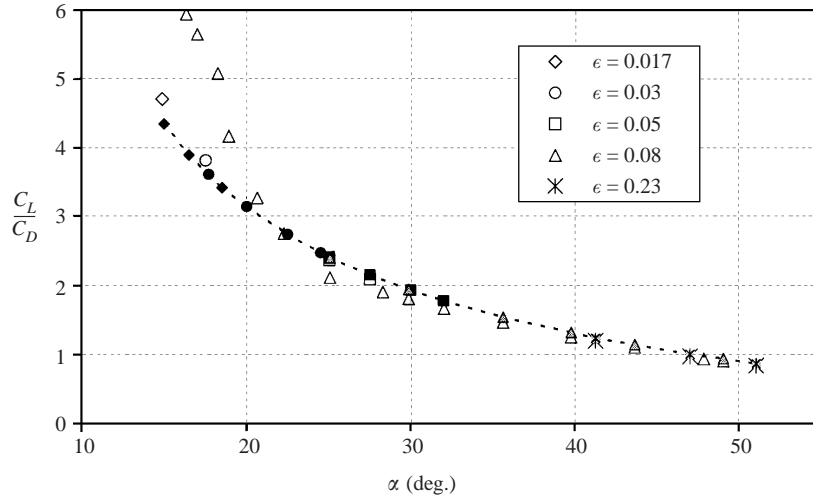


FIGURE 10. Comparison of aerodynamic coefficients between computed (solid symbols) ($\epsilon = 0.08$ and 0.23) and experimental (open symbols) results obtained by Newman & Low (1984) ($\epsilon = 0.017$, 0.03 and 0.05).

computed values of C_L/C_D for any excess length ratio ϵ all lie on a same curve:

$$\frac{C_L}{C_D} = -10^{-7}\alpha^5 + 2.10^{-5}\alpha^4 - 0.0018\alpha^3 + 0.0701\alpha^2 - 1.5012\alpha + 15.991, \quad (4.1)$$

where α is the incidence of the sail in degrees. Very good agreement is shown between the different experimental results for the different sails. The experimental and numerical data differ in the values of the lift or the drag coefficient only because of the Helmholtz wake assumption ($C_p = 0$). It is thus possible to say that the inaccuracies in the approximation of the forces (lift, drag and tension) are due only to the assumed null pressure coefficient in the wake. For fully separated flows, this approximation affects the lift and drag coefficients the same way: C_L/C_D is well approximated.

Newman & Low (1984) and Cyr & Newman (1996) presented experimental and numerical results for separation points on the sail without bubbles at the leading edge (design incidence). These authors give the position of the separation point on the sail, which must be known for our numerical method, so comparison is possible. As has been said previously, the aerodynamic forces are not well predicted. So, the comparison is made for the sail shape and especially on the angles at the leading and trailing edges (figure 11): $\theta_L = \pi - \beta_1 + \alpha$ and $\theta_T = \beta_N$ (figure 1). The results are in relatively good agreement for the leading edge and differ a little more for the trailing edge. It should be pointed out that the results are not very different from the theory of Thwaites (1961). Nevertheless, the maximum camber and its position differ more for this theory. For fully separated flows, the functions θ_L/α and θ_T/α , the maximum camber and its position depend only on the parameter $\alpha/\sqrt{\epsilon}$.

To validate the calculations for configurations with a mast, we performed experiments and explored the flow around the sail by PIV.

4.4. More general configurations

Many different experimental configurations have been studied in the Lucien Malavard wind tunnel in Orléans (table 2). Different parameters (c_m , c , L , ϕ , α and Re) were

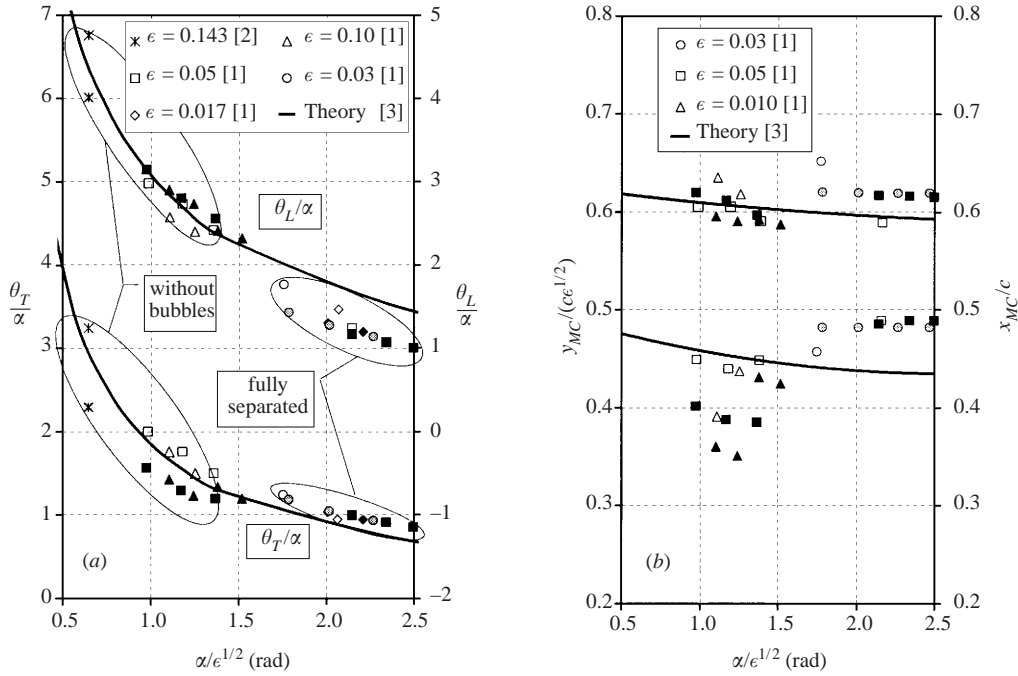


FIGURE 11. (a) Comparison of leading and trailing edge angles and (b) camber ratio and position of maximum camber between experiments (open symbols: [1] Newman & Low (1984) and [2] Cyr & Newman (1996)), theory ([3] Thwaites (1961)) and computed values (solid symbols). Separation point on the sail.

	Mast			Sail			Flow Re
	Profile	c_m (mm)	ϕ (deg.)	L (mm)	c (mm)	α (deg.)	
Config. 1 PIV	NACA0060	28	16	479	458	6	4.6×10^5
			-17			20	
			30				
			-30				
Config. 2 PIV	NACA0060	28	-8	490	445	29	1.5×10^5
							3×10^5
							4.5×10^5
			13			11.5	1.6×10^5
							3.1×10^5
Config. 3 PIV	NACA0060	60	-6	1104	892	31	3.6×10^5
			41			41	3.4×10^5
			37			27.6	2.3×10^5
Config. 4 PIV + Bal.	NACA0040	33	-2.5	324	300	2.7-49	0.88×10^5
						265	41.2-51

TABLE 2. Experimental configurations.

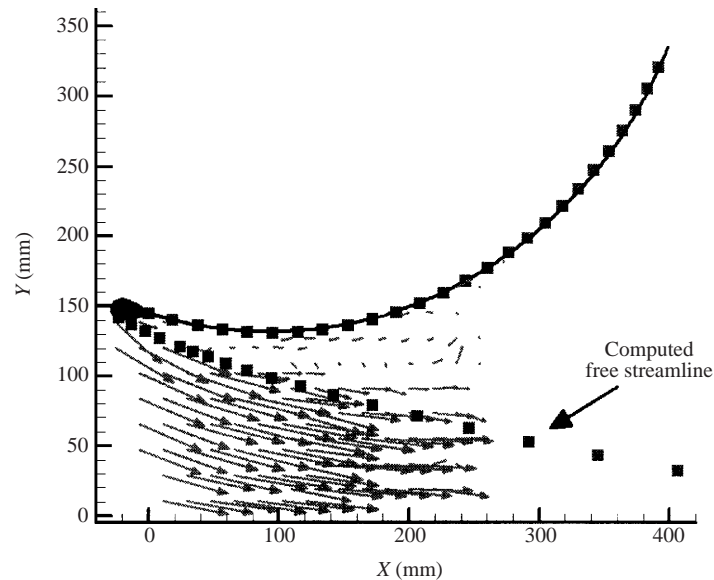


FIGURE 12. Velocity field and sail shapes with a separation point on the mast ($\phi = 8^\circ$, $c = 445$ mm, $L = 490$ mm, $\alpha = 29^\circ$ and $Re = 1.5 \times 10^5$). The symbols represent the computed free streamline and sail, and the line the experimental sail.

varied to change the position of the separation point and obtain fully separated (separation on the mast), partially separated (separation on the sail) or attached flows. The Reynolds number Re is based on the sail chord c . Three of these configurations are presented here.

We first consider a case where the separation point is located on the mast (configuration 2 of table 2): $\phi = 8^\circ$, $c = 445$ mm, and $\alpha = 29^\circ$ ($\epsilon = 0.1$). The uniform infinite velocity is $V_\infty = 5 \text{ m s}^{-1}$ ($Re = 1.5 \times 10^5$). The PIV visualization window is about 150×150 mm, which corresponds to an interrogation area of 2.5×2.5 mm with the chosen resolution. The time delay between two illuminations is $60 \mu\text{s}$. The post-processing used here is very simple. It consists in averaging sixty instantaneous velocity fields and applying a velocity range filter. Good agreement can be seen between the computed and experimental shapes (figure 12). Moreover, the free streamline geometry is quite satisfactory as it corresponds to the jump between high and low velocities.

The next case is one in which the separation point is on the sail (configuration 2 of table 2): $\phi = 13^\circ$, $c = 469$ mm, $\alpha = 11.5^\circ$ ($\epsilon = 0.05$), and $Re = 3.1 \times 10^5$. The velocity field is recorded in three views of 180×180 mm, with interrogation areas of 2.5×2.5 mm. The computed shape is still close to the experimental one, and the free streamline geometry is anticipated with good accuracy (figure 13).

The third configuration (figure 14) is one of near-attached flow (the separation point is far from the mast). This is configuration 4 of table 2 ($\phi = -2.5^\circ$, $c = 300$ mm, $\alpha = 2.7^\circ$ ($\epsilon = 0.08$), and $Re = 0.88 \times 10^5$). Again, the correspondence between the results is good.

5. Conclusion

Our numerical method solves the problem of two-dimensional separated flows past flexible sails. We use a recursive scheme which solves the problem in two main steps.

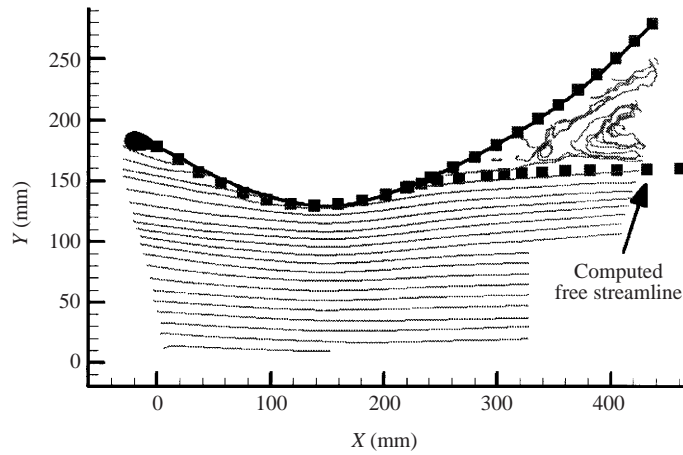


FIGURE 13. Experimental streamlines and sail shapes with a separation point on the sail ($\phi = 13^\circ$, $c = 469$ mm, $L = 490$ mm, $\alpha = 11.5^\circ$ and $Re = 3.1 \times 10^5$). The symbols represent the computed free streamline and sail, and the line the experimental sail.

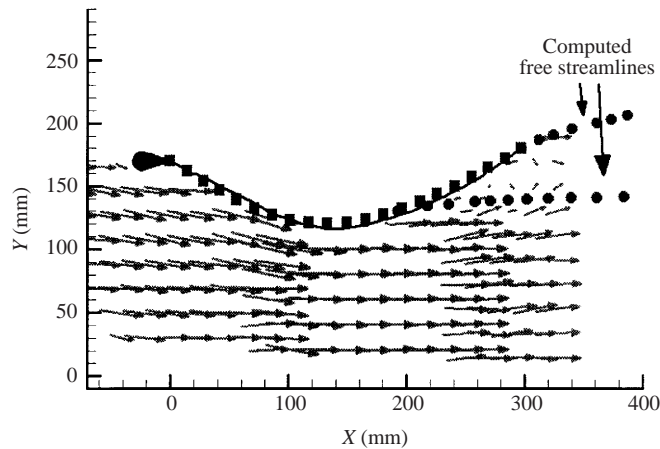


FIGURE 14. Velocity field and sail shapes with a separation point on the sail far from the mast ($\phi = -2.5^\circ$, $c = 300$ mm, $L = 325$ mm, $\alpha = 2.7^\circ$ and $Re = 0.88 \times 10^5$). The symbols represent the computed free streamline and sail, and the line the experimental sail.

First, the pressure distribution on the assumed rigid sail is computed by solving a Dirichlet problem on the unit circle. Then the sail is deformed to reach a static equilibrium condition. Convergence is reached after a few dozen iterations, requiring a computation time ranging from a few seconds to five minutes on a PC 500 MHz.

This numerical method was validated with experimental data generated by PIV instrumentation. We found close agreement between experimental and numerical data for the sail shape and for the free streamline geometry. This was surprising since we knew that the Helmholtz model does not predict global forces correctly for large wakes. In fact, $Cp = 0$ in the wake is a poor approximation for such cases. This might explain why the agreement seems to be better in the second case (with separation on the sail) than in the first (separation on the mast). As the results on the lift and drag coefficient do not agree with experimental data, we will apply some other wake model to our method, such as the virtual wall model introduced by Joukowski and

developed by Roskho (1954) and Wu & Wang (1964). This model considers the wake to be an infinite dead flow area with an unknown constant pressure $P_0 \neq P_\infty$, which is possible with two horizontal semi-infinite flat plates whose position is an unknown (Toison 1998).

These experiments were useful not only in validating our computations, but also in determining the physical position of the separation points. These positions need to be known in order for the numerical method to work, and they greatly affect the shape of the sail and consequently the different forces. Since the general method seems to yield good results in comparison with experiment, we intend to couple this method with a boundary layer model in order to predict the position of the separation point. This will, of course, increase computation time; but since the purpose here is to solve the rigid sail on the unit semi-circle (solution of (2.19)), there is no need to converge the whole problem since the separation point is not well positioned. The usefulness of the approach presented (which predicts sail shape well and the forces quite well with a few minutes calculation on a PC) should be confirmed.

Our method will also be extended to the flow past interacting flexible sails. This will imply solving a mixed-boundary problem with four zones on the unit-circle, and the same deformation method will be applied. We are also considering PIV experiments, since the existing data for such a case (Myall & Berger 1969) are all based on a fully attached flow.

REFERENCES

- BAILEY, K. I., JACKSON, P. S. & FLAY, R. G. J. 1998 Modelling viscous flow around 2D yacht mast and sail configurations. *Proc. 1998 13th Australasian Fluid Mech. Conf., Melbourne, Australia*, pp. 519–522.
- BARAKAT, R. 1968 Incompressible flow around porous two-dimensional sails and wings. *J. Maths & Phys.* **47**, 327–349.
- BUNDOCK, M. S. 1980 *Aerodynamics of two-dimensional sail wings*. MSc Dissertation, University of Waikato.
- CISOTTI, V. 1932 Moto con scia di un profilo flessibile. *Accad. Nat. Dei Lincei* **15**, 116–173.
- CYR, S. & NEWMAN, B. G. 1996 Flow past two-dimensional membrane aerofoils with rear separation. *J. Wind Engng Ind. Aero.* **63**, 1–16.
- DUGAN, J. P. 1970 A free-streamline model of the two-dimensional sail. *J. Fluid Mech.* **42**, 433–446.
- FITT, A. D. & LATTIMER, T. R. B. 2000 On the unsteady motion of two-dimensional sails. *IMA J. Appl. Maths* **65**, 147–171.
- GREENHALGH, S., CURTISS, H. C. & SMITH, B. 1984 Aerodynamic properties of a two-dimensional inextensible flexible airfoil. *AIAA J.* **22**, 865–870.
- GUREVICH, M. I. 1966 *Theory of Jets in an Ideal Fluid*. Pergamon.
- HUREAU, J., BRUNON, E. & LEGALLAIS, PH. 1996 Ideal free streamline flow over a curved obstacle. *J. Comput. Appl. Maths* **72**, 193–214.
- HUREAU, J. & WEBER, R. 1998 Impinging free jets of ideal fluid. *J. Fluid Mech.* **372**, 357–374.
- IRVINE, H. M. 1979 A note on luffing in sails. *Proc. R. Soc. Lond. A* **365**, 345–347.
- JACKSON, P. S. 1983 A simple model for elastic two-dimensional sails. *AIAA J.* **21**, 153–155.
- JACKSON, P. S. 1984 Two-dimensional sails in invicid flow. *J. Ship Res.* **28**, 11–17.
- JACKSON, P. S. & CHRISTIE, G. W. 1987 Numerical analysis of three-dimensional elastic membrane wings. *AIAA J.* **25**, 676–682.
- LEGALLAIS, PH. & HUREAU, J. 1994 Singularity method applied to the classical Helmholtz flow coupling procedure with boundary layer calculation. *J. Phys. Paris III* **4**, 1053–1068.
- LÉVI-CIVITA, T. 1907 Scie e leggi di resistenza. *Rend. Circolo Math. Palermo* **23**, 1–37.
- LILLBERG, E., KAMAKOTI, R. & SHYY, W. 2000 Computation of unsteady interaction between viscous flows and flexible structure with finite inertia. *AIAA Paper* 2000–0142.
- MILNE-THOMSON, L. M. 1968 *Theoretical Hydrodynamics*, 5th Edn. Macmillan.

- MURAI, H. & MARUYAMA, S. 1980 Theoretical investigation of the aerodynamics of double membrane sailing airfoil sections. *J. Aircraft* **17**, 294–299.
- MURATA, S. & TANAKA, S. 1989 Aerodynamic characteristics of a two-dimensional porous sail. *J. Fluid Mech.* **206**, 463–475.
- MUSKHELISHVILI, N. I. 1977 *Singular Integral Equations*, 5th Edn. Noordhoff.
- MYALL, J. O. & BERGER, S. A. 1969 Interaction between a pair of two-dimensional sails for the case of smoothly attached flow. *Proc. R. Soc. Lond. A* **310**, 373–391.
- NEWMAN, B. G. 1987 Aerodynamic theory for membranes and sails. *Prog. Aerospace Sci.* **24**, 1–27.
- NEWMAN, B. G. & LOW, H. T. S. 1981 Two-dimensional flow at right angles to a flexible membrane. *Aeronaut. Q.* **32**, 243–269.
- NEWMAN, B. G. & LOW, H. T. S. 1984 Two-dimensional impervious sails: experimental results compared with theory. *J. Fluid Mech.* **144**, 445–462.
- NIELSEN, J. N. 1963 Theory of flexible aerodynamic surfaces. *Trans. ASME: J. Appl. Mech.* **30**, 435–442.
- ROBERT, J. & NEWMAN, B. G. 1979 Lift and drag of a sail aerofoil. *Wind Engng* **3**, 1–22.
- ROSKHO, A. 1954 A new hodograph for free streamline flow theory. *NACA TN* 3168.
- SMITH, R. & SHYY, W. 1995a Computational model of a flexible membrane wings in steady laminar flow. *AIAA J.* **37**, 1769–1777.
- SMITH, R. & SHYY, W. 1995b Computation of unsteady laminar flow over a flexible two-dimensional membrane wing. *Phys. Fluids* **7**, 2175–2184.
- SMITH, R. & SHYY, W. 1996 Computation of aerodynamic coefficients for a flexible membrane airfoil in turbulent flow: a comparison with classical theory. *Phys. Fluids* **8**, 3346–3353.
- SMITH, R. & SHYY, W. 1997 Incremental potential flow based membrane wing element. *AIAA J.* **33**, 782–788.
- SNEYD, A. D. 1984 Aerodynamic coefficients and longitudinal stability of sail aerofoils. *J. Fluid Mech.* **149**, 127–146.
- STEWART, H. J. 1942 A simplified two-dimensional theory of thin airfoils. *J. Aero. Sci.* **9**, 452–456.
- SUGIMOTO, T. 1996 A theory of inextensible and high aspect-ratio sails. *J. Wind Engng Ind. Aero.* **63**, 61–75.
- THWAITES, B. 1961 The aerodynamic theory of sails. I. Two-dimensional sails. *Proc. R. Soc. Lond. A* **261**, 402–422.
- TOISON, F. 1998 Validation d'une méthode numérique générale de calcul d'écoulements bidimensionnels de fluide parfait. Application aux sillages épais et aux surfaces libres avec effet de la gravité. PhD Thesis, Université Orléans.
- TOISON, F. & HUREAU, J. 2000 Open-channel flows and waterfalls. *Eur. J. Mech. B/Fluids* **19**, 269–283.
- TUCK, E. O. & HASEL GROVE, M. 1972 An extension of two-dimensional sail theory. *J. Ship Res.* **16**, 148–152.
- VANDEN-BROECK, J. M. 1982a Nonlinear two-dimensional sail theory. *Phys. Fluids* **25**, 420–423.
- VANDEN-BROECK, J. M. 1982b Contact problems involving the flow past an inflated aerofoil. *Trans. ASME: J. Appl. Mech.* **49**, 263–265.
- VANDEN-BROECK, J. M. & KELLER, J. B. 1981 Shape of a sail in a flow. *Phys. Fluids* **24**, 552–553.
- VOELZ, K. 1950 Profil und Auftrieb eines Segels. *Z. Angew. Math. Mech.* **30**, 301–317.
- WEBER, R. & HUREAU, J. 2001 Ideal fluid flow past obstacles in an arbitrary channel. Comparison of numerical and experimental results. *J. Fluid Mech.* **447**, 129–148.
- WILKINSON, S. 1988 Simple multilayer panel method for partially separated flows around two-dimensional masts and solids. *AIAA J.* **26**, 394–395.
- WU, T. Y. & WANG, D. P. 1964 A wake model for free streamline flow theory. *J. Fluid Mech.* **18**, 65–93.